Journal of Magnetic Resonance 209 (2011) 61–68

Contents lists available at ScienceDirect

Journal of Magnetic Resonance

journal homepage: www.elsevier.com/locate/jmr

Coherence times and Rabi oscillations in $CaWO_4$:Cr^{5+} crystal

Eduard Baibekov [a,*], Igor Kurkin [a], Marat Gafurov [a,b], Burkhard Endeward [b], Rafail Rakhmatullin [a], Georgy Mamin [a]

[a] Kazan Federal University, 420008 Kazan, Russian Federation, Russia
[b] Institute of Physical and Theoretical Chemistry, Centre of Biomolecular Magnetic Resonance, Goethe University, 60438 Frankfurt am Main, Germany

ARTICLE INFO

Article history:
Received 4 November 2010
Revised 30 December 2010
Available online 4 January 2011

Keywords:
Pulsed ESR
Calcium tungstate
Pentavalent chromium
Rabi oscillations
Inhomogeneous fields

ABSTRACT

The coherence times of dopant pentavalent chromium ions in $CaWO_4$ single crystal (0.0006 at.% Cr^{5+}) were investigated both theoretically and experimentally. Temperature dependences of spin–lattice relaxation time T_1 and phase memory time T_M were measured in the temperature range 6–30 K at high (94 GHz, *W* band) and low (3.5 GHz, *S* band) frequencies of electron spin resonance. It follows from T_M calculations that phase relaxation of Cr^{5+} ion arises mainly from magnetic dipole interactions between the chromium ions.

Anomalously fast damping of Rabi oscillations is detected in both *S*- and *W*-band experiments. It is shown that this phenomenon is caused by microwave field inhomogeneity inside the resonator. Relations between the damping time of Rabi oscillations, Rabi frequency and the crystal sample size are obtained. Lumped-element resonators and smaller sample dimensions are suggested to lower spin dephasing during transient nutations.

1. Introduction

The fundamental obstacle to successful implementation of a quantum computer is decoherence problem [1]. The quantum bits (qubits) must be put into such environment that their behavior is coherent while they are manipulated during quantum computation process. One possible realization of qubit is an electron spin operable with the application of magnetic field flipping pulses [1–3].

Recently, paramagnetic ions diluted in diamagnetic solid matrices have been proposed as possible qubit implementations, namely, rare earth [4–6] and transition metal ions [7–11]. The spin manipulation in such systems is achieved by application of short microwave (MW) pulses as part of electron spin resonance (ESR) experiments. Due to highly elaborated experimental techniques available in the field of magnetic resonance and relatively short qubit switching times such implementations are advantageous.

One of the most famous effects in magnetic resonance where quantum coherence manifests itself is the electron spin-echo (ESE) phenomenon. The resultant echo amplitude is lessened by irreversible loss of magnetization during the time between and after the pulses of the spin-echo sequence (i.e., in the absence of MW magnetic field). Here the time of application of resonant MW field is limited by the duration of the pulse, which is much less than phase coherence time T_M. In case of sufficiently small dopant concentrations, T_M can exceed 100 μs, along with the number of coherent single-qubit operations Q_M reaching 10^4 [6].

In quantum computation, one needs to apply sufficient amount of successive MW pulses. Thus, apart from T_M, it is crucial to know the spin coherence time during the spin transient nutation. The measure of such coherence is the damping time τ_R of so-called Rabi oscillations (or transient nutations) [12]. These are quantum oscillations resulting from coherent absorption and emission of photons under the application of a long resonant MW pulse. The number of coherent single-qubit operations is defined as $Q_M = \Omega_R T_M/\pi$, where Ω_R is Rabi frequency. Up to now, there is a considerable number of publications indicating anomalously fast damping of Rabi oscillations (RO) of paramagnetic impurities diluted in crystal matrices. Probably the first observations were carried out for *E′*-centers in glassy silica and for $[AlO_4]^0$ centers in quartz [13–15]. They revealed the peculiar linear dependence of τ_R^{-1} on Ω_R:

$$\tau_R^{-1} = \frac{1}{2}T_M^{-1} + \beta\Omega_R, \tag{1}$$

with the dimensionless coefficient $\beta \sim 10^{-2} \div 10^{-1}$. Apart from [13–15], the anomalous damping of RO was observed recently in Er^{3+}-doped [4,5] and Yb^{3+}-doped [6] $CaWO_4$ crystals, in molecular magnets Fe_4 [8] and V_{15} [9,10], in MgO:Mn^{2+} [7] and in K_3NbO_8:Cr^{5+} [11]. For ordinary experimental conditions, the second term in (1) prevails over the first one. For appropriate MW field intensities, the ratio T_M/τ_R may be as high as 10^3 [6]. The term $T_M^{-1}/2$ is explained in the framework of Bloch model [13]. However, to the

* Corresponding author.
E-mail address: edbaibek@gmail.com (E. Baibekov).

1090-7807/$ - see front matter © 2011 Elsevier Inc. All rights reserved.
doi:10.1016/j.jmr.2010.12.015

best of our knowledge, there is still no satisfactory explanation of the term linear in Ω_R, except, perhaps, the stochastic semi-phenomenological model developed in [14,15]. Another distinctive feature of RO is its decay pattern which is usually weaker than exponential, containing tens of residual oscillations [4,6]. The damping of transient nutations might in principle indicate some decoherence process occurring in the presence of resonant MW field, and that would lead to sufficient reduction of Q_M in the system under consideration.

In the present work we report an extensive study of coherence dynamics in $CaWO_4$:Cr^{5+} crystal at high-frequency W band (94 GHz) and low-frequency S band (3.5 GHz) ESR. Firstly, we present temperature dependences of spin–lattice relaxation time T_1 and phase memory time T_M of Cr^{5+} ion and discuss the possible relaxation pathways that lead to the particular $T_1(T)$ and $T_M(T)$ dependences. Secondly, we observe RO and both qualitatively and quantitatively explain the mechanism of their anomalous decay as the result of MW field inhomogeneity over the crystal sample volume.

2. Results and discussion

$CaWO_4$ crystal has scheelite structure with lattice constants $a = 5.243$ Å, $c = 11.374$ Å [16]. The Cr^{5+} ions substitute for W^{6+} ions at sites with S_4 point symmetry [17]. The ground state of the only $3d$ electron on the outer shell of the Cr^{5+} ion is predominantly $3d_{z^2}$ orbital ($z||c$) forming a Kramers doublet with almost isotropic g tensor ($g_\parallel = 1.989$, $g_\perp = 1.945$ [17,18]). Our crystal field calculations based on Exchange Charge Model [19] suggest also that the ground state is separated from the next upper energy level by the gap of nearly 4000 cm^{-1}. Thus, even at room temperature, we can regard a single Cr^{5+} ion in $CaWO_4$ crystal as a two-level system suitable for qubit implementation, the degeneracy being removed by the application of external magnetic field.

An example of an echo-detected ESR spectrum of the Cr^{5+} ion in $CaWO_4$ crystal at S band is shown in Fig. 1. An intense central line at 1297 G corresponds to even isotopes of Cr^{5+} ion with nuclear spin $I = 0$, four hyperfine satellites are from odd isotope $^{53}Cr^{5+}$ ($I = 3/2$, natural abundance 9.55%).

2.1. Spin–lattice relaxation time T_1

Fig. 2 shows the temperature dependence of T_1^{-1} measured at the central line at S band ($T = 3$–15 K) and at W band ($T = 6$–30 K). One can distinguish between several possible contributions into T_1^{-1}. Firstly, it is a contribution from direct relaxation processes, $T_{1d}^{-1} = AT$, where the parameter A is essentially frequency-dependent [20]. In our case direct processes are apparently negligible at least at $T > 6$ K since T_1^{-1} dependences for both ESR bands coincide in the range of 6–15 K. Secondly, it is a contribution from Raman relaxation processes which, if calculated in the framework of Debye model of the phonon spectrum, gives rise to $T_{1R}^{-1} = CT^9$ term. A rough estimate according to [20] gives $C \simeq 1.4 \times 10^{-7}$ s^{-1} K^{-9}. Both contributions mentioned above describe very well the $T_1^{-1}(T)$ dependence for the isostructural $CaMoO_4$:Cr^{5+} crystal [21], with $A = 8 \times 10^{-2}$ s^{-1} K^{-1}, $C = 1.67 \times 10^{-7}$ s^{-1} K^{-9}. However, the form of $T_1^{-1}(T)$ dependence for $T > 4$ K in $CaWO_4$:Cr^{5+} is somewhat different from [21], resembling rather exponential than polynomial dependence on T. It may be explained by the fact that Debye model is inadequate in the case of $CaWO_4$ crystal, as it was shown in [22]. More accurate estimates of T_{1R}^{-1} require elaborate computations of the low-frequency optical phonon modes which are beyond the scope of this work. We have found that $T_1^{-1}(T)$ in $CaWO_4$:Cr^{5+} may be well approximated by the following function (solid line in Fig. 2):

$$T_1^{-1}(T) = AT + B_1 e^{-\frac{\Delta_1}{k_B T}} + B_2 e^{-\frac{\Delta_2}{k_B T}}, \quad (2)$$

with $A = 0.3$ s^{-1} K^{-1}, $B_1 = 3 \times 10^6$ s^{-1}, $\Delta_1 = 39$ cm^{-1}, $B_2 = 1.5 \times 10^8$ s^{-1}, $\Delta_2 = 83$ cm^{-1}. The 2nd and 3rd terms in (2) resemble contributions from Orbach processes [20]. However, that will require the existence of two upper electronic sublevels with energies 39 and 83 cm^{-1}, which is extremely unlikely since the energy gap between the ground state and the next upper state of Cr^{5+} ion is estimated ~4000 cm^{-1}. Instead, these terms apparently relate to some peaks in the crystal's phonon density of states (PDS). The PDS of $CaWO_4$ computed in [22] shows a maximum near Δ_2. As for Δ_1, a corresponding maximum in PDS may arise from local lattice perturbations due to activation of the crystal with Cr^{5+} ions.

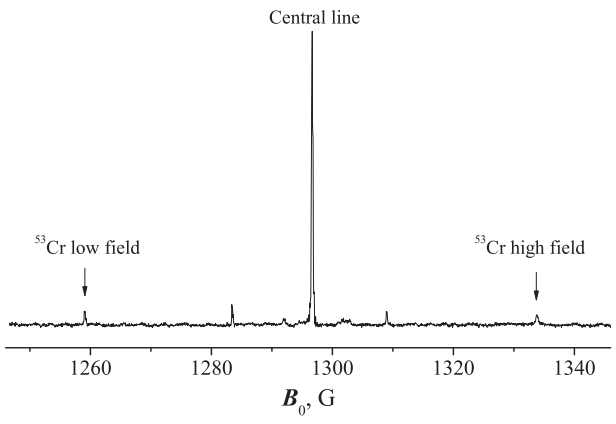

Fig. 1. Field-swept echo-detected ESR spectrum of Cr^{5+} ion in $CaWO_4$ crystal at resonance frequency 3.53 GHz (S band) showing well-separated central line and four hyperfine satellites. $T = 5$ K, $\boldsymbol{B}_0 \perp c$.

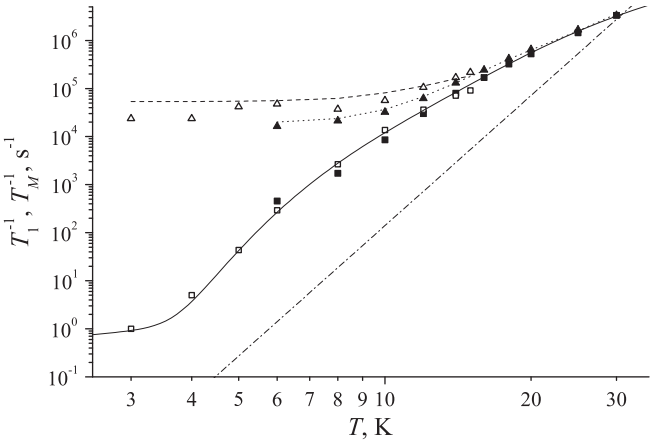

Fig. 2. Temperature dependence of spin–lattice (T_1^{-1}, squares) and phase (T_M^{-1}, triangles) relaxation rates measured at the central ESR line of Cr^{5+} ion in $CaWO_4$ crystal. Data are collected in S band (open symbols) and in W band (solid symbols). Solid line is the fit of T_1^{-1} to Eq. (2). Dashed and dotted lines represent results of T_M^{-1} calculations (Eq. (3)) in S and W bands, respectively. The dash-dotted line represents 1.4×10^{-7} T^9 dependence. $\boldsymbol{B}_0, \boldsymbol{B}_1 \perp c$.

2.2. Phase memory time T_M

The temperature dependence $T_M(T)$ for the central ESR line measured in the range of 3–30 K is presented in Fig. 2. The interpretation of T_M times will be given here in accord with the existing model of phase relaxation of magnetic impurities diluted in diamagnetic matrices [23,24]. The phase relaxation of Cr^{5+} ions in $CaWO_4$ crystal is attributed to the fluctuations of local magnetic fields at the sites of magnetic ions. In turn, local magnetic fields at Cr^{5+} sites are induced by various interactions:

1. The short-range exchange interactions between Cr^{5+} ions. Since the average Cr–Cr distance in our crystal sample exceeds 200 Å, these interactions are negligible.
2. Superhyperfine interactions between Cr^{5+} ions and magnetic nuclei in the crystal lattice. However, the only magnetic nuclei in the host matrix (^{183}W) are of minor importance due to their low natural abundance (14%) and low magnetic moments (0.117 nuclear magnetons).
3. The magnetic dipole (MD) interactions between Cr^{5+} ions that cause static broadening of ESR line with the half-width $\Delta\omega_d = \frac{4\pi^2}{9\sqrt{3}\hbar} C g_\perp^2 \mu_B^2$ [23], where C is the concentration of Cr^{5+} ions and μ_B is Bohr magneton. For our crystal sample, $\Delta\omega_d = 6 \times 10^4\ s^{-1}$. It is natural therefore to confine ourselves only to MD interactions as the main source of phase decoherence in $CaWO_4$:Cr^{5+} crystal. In turn, MD interactions between Cr^{5+} ions result in two mechanisms of decoherence: spectral diffusion (SD) and instantaneous diffusion (ID) [24].

In the case of ID, the fluctuations of local magnetic fields are induced by spin flips caused by $\pi/2$ and π pulses in ESE pulse sequence. Due to crystal defects and local magnetic fields, ESR lines of paramagnetic centers in solids are inhomogeneously broadened. The spin-echo sequence in T_M measurements is used to get rid of static local magnetic fields. However, the Cr^{5+} ions that have their Larmor precession frequencies close to resonance undergo rotations, and thus their contribution to the local magnetic fields is essentially nonstatic and varies during the ESE experiment. Roughly only the Cr^{5+} ions with Larmor precession frequencies detuned from resonance by values of order $\Omega_R = g_\perp \mu_B B_1/(2\hbar)$ contribute to such fluctuations (B_1 being the amplitude of linearly polarized microwave field, $\boldsymbol{B}_1 \perp c$). The corresponding relaxation rate is given by the expression $\kappa\Delta\omega_d\langle\sin^2(\theta_2/2)\rangle$ [24]. Here κ is the fraction of Cr^{5+} ions corresponding to the given ESR line (for the central ESR line, $\kappa = 0.9$), θ_2 is the spin nutation angle during the second (π) pulse in ESE sequence, $\langle\ldots\rangle$ denotes averaging over the distribution of Larmor frequencies of Cr^{5+} ions in the ESR line. For $\Omega_R < \sigma$ (2σ being the inhomogeneous ESR linewidth), the ESR line is only partially excited, so $\langle\sin^2(\theta_2/2)\rangle < 1$.

In the case of SD, the fluctuations of local magnetic fields are attributed to spin flips induced (1) by the spin–lattice interaction and (2) by MD interaction (flip-flop processes). When $T_1^{-1} < \Delta\omega_d$, the contribution of the former process into T_M^{-1} is estimated as $\sqrt{T_1^{-1}\Delta\omega_d}/2$ [24] and thus is independent of Ω_R/σ. The latter process is of importance when the energy of MD interaction between a pair of spins is comparable to the difference between their Larmor frequencies. Since the ratio $\Delta\omega_d/\sigma \ll 1$ for our crystal sample, we neglect mutual spin flip-flops. Thus, one obtains the following formula for the phase relaxation rate T_M^{-1} of Cr^{5+} ion in $CaWO_4$:

$$T_M^{-1} = \kappa\Delta\omega_d\left\langle \sin^2\frac{\theta_2}{2}\right\rangle + \frac{1}{2}\sqrt{T_1^{-1}\Delta\omega_d} + T_1^{-1}, \tag{3}$$

where the last term corresponds to the direct contribution to T_M^{-1} from the spin–lattice relaxation. Note that Eq. (3) contains no phenomenological parameters of any sort. Given C, $g_\perp$, T_1 and the ESR line profile, the phase memory time calculations are straightforward. The dependences of $T_M^{-1}(T)$ thus obtained agree very well with experimental results for both S and W bands (see Fig. 2). As shown in Fig. 2, the spin–lattice relaxation has almost no effect on phase relaxation of Cr^{5+} at temperatures below 10 K, where T_M^{-1} is independent of T. There, due to low T_1^{-1} values, both the 2nd and the 3rd terms in (3) become relatively small. The main contribution there is ID, which has another evidence: ESE envelopes measured in that temperature region are exponential $\sim\exp(-2\tau/T_M)$ (characteristic of ID) rather than Gaussian (SD). It means that if we lower the dopant Cr^{5+} concentration, we can achieve even longer phase memory times in the system under consideration. This is strongly supported by the fact that measured T_M time of odd Cr^{5+} isotopes with essentially smaller concentration κC in the same crystal sample reached 0.2 ms. The observed discrepancy by a factor of 3 between T_M^{-1} values for S and W bands near $T = 6$ K is due to the differences in the lengths of $\pi/2$ pulses for both bands and inhomogeneous widths of ESR lines (0.25 G and 10 G for S and W band, respectively), which affect the number of spins driven by the MW pulse and, consequently, the value of $\langle\sin^2(\theta_2/2)\rangle$ in Eq. (3).

2.3. Decay of Rabi oscillations

Some of the measured RO are presented in Fig. 3 (W band) and Fig. 4A (S band). As in recent papers [4–11,13–15], the observed RO decay rates exceeded both T_1^{-1} and T_M^{-1} values and depended linearly on Rabi frequency. In order to give theoretical interpretation of this anomalous decay, we perform direct calculation of RO in the presence of strong inhomogeneous broadening of ESR line and MW magnetic field distribution inside the resonator.

Firstly, we take into account the damping of average magnetization due to inhomogeneous broadening of ESR line. We consider a typical situation of strong broadening, when the line width exceeds the nutation frequency, i.e. $\sigma > \Omega_R$. It means that only a part of Cr^{5+} ions contained in the crystal sample is involved in transient nutations. We assume that at $t = 0$, when the linearly polarized MW magnetic field $B_1 \cos\omega_0 t$ is turned on, the average magnetization is parallel to $\boldsymbol{B}_0$. Then we introduce reference frame rotating around the direction of $\boldsymbol{B}_0$ with frequency ω_0. There the magnetization $\boldsymbol{S}(\varepsilon, t)$ of a single spin packet detuned from resonance by $\varepsilon = \omega - \omega_0$ rotates at frequency $f(\varepsilon) = \sqrt{\Omega_R^2 + \varepsilon^2}$, and its projection $S_{||}(\varepsilon, t)$ along $\boldsymbol{B}_0$ is [25]:

$$S_\parallel(\varepsilon, t) \sim \frac{\Omega_R^2\cos(ft) + \varepsilon^2}{\Omega_R^2 + \varepsilon^2}. \tag{4}$$

Let us perform the averaging over the spectral position of Cr^{5+} ion in ESR line, i.e. integrate over the ESR line shape $g(\varepsilon)$. Since $\sigma > \Omega_R$, we assume $g(\varepsilon) \approx g_0$ and extend the integration limits to infinity:

$$\langle S_\parallel(t)\rangle = \int g(\varepsilon) S_\parallel(\varepsilon, t) d\varepsilon \simeq g_0 \int_{-\infty}^{\infty} S_\parallel(\varepsilon, t) d\varepsilon \sim j_0(\Omega_R t), \tag{5}$$

where we have neglected the term independent of t in Eq. (4); $j_0(v)$ in Eq. (5) is the integral from zeroth-order Bessel function $J_0(v)$:

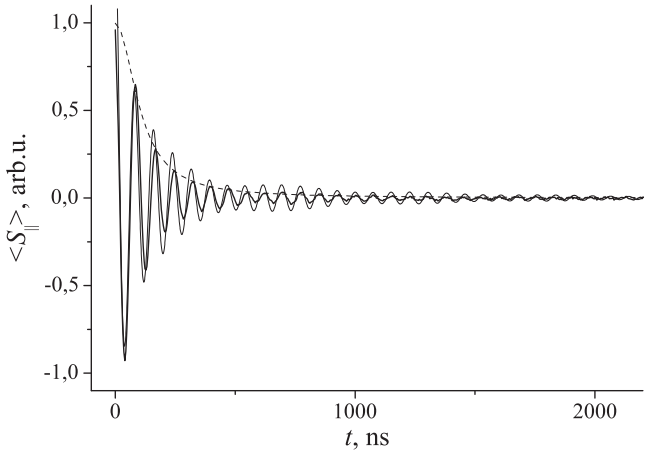

Fig. 3. Rabi oscillations obtained at the central ESR line of W band. $\Omega_R = 8 \times 10^7\ s^{-1}$. $T = 6$ K. Experimental data, the results of calculations, and the fit to the Lorentzian $\langle S_{||}(0)\rangle(1 + (t/\tau_R)^2)^{-1}$ are represented by thick solid, thin solid and dashed lines, respectively.

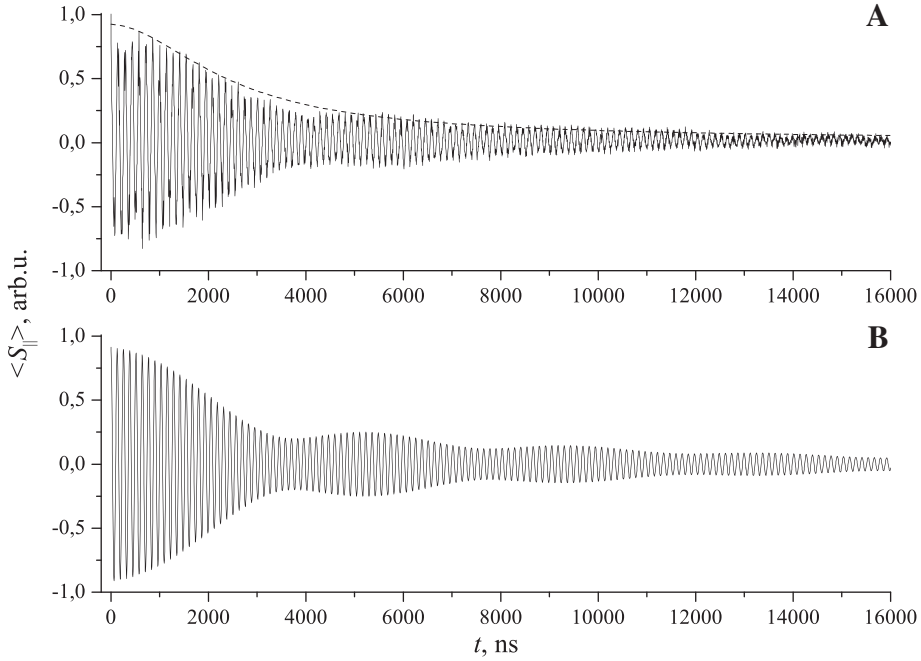

Fig. 4. Rabi oscillations obtained at the central ESR line of *S* band. $\Omega_R = 5 \times 10^7\ s^{-1}$, $T = 5$ K. A – experimental data (solid line) and the fit to $\langle S_{\|}(0)\rangle e^{-\kappa\Delta\omega_d t/2}(1+(t/\tau_R)^2)^{-3/4}$ with $\tau_R = 2.2$ μs (dashed line). B – the results of calculations assuming 96% MW magnetic field homogeneity inside the crystal sample.

$$j_0(v) = \int_v^\infty J_0(v')dv'.$$

Using an asymptotic representation of Bessel function, we derive the approximate formula:

$$j_0(v) \simeq \sqrt{2}(1+(\pi v)^2)^{-1/4}\cos\left(v+\frac{\pi}{4}\right), \tag{6}$$

which is a good approximation when $v \gg 1$ and a very rough one when $v \sim 1$.

Secondly, we take into account the MW magnetic field distribution inside the resonator. It is formed by standing waves of MW field inside the rectangular or cylindrical resonant cavity. The role of MW field inhomogeneity in the damping of Rabi oscillations is indicated in [26,27]. However, to the best of our knowledge, there is still no quantitative description of the effect, i.e. the dependence of the corresponding damping time on the crystal sample size, resonator type and Rabi frequency. Note also that this effect was neglected in Refs. [4–11]. We start with the transverse electric TE_{011} cylindrical mode commonly used in ESR spectroscopy. In cylindrical coordinates (ρ, z, φ), the components of the amplitude vector $\boldsymbol{B}_1$ of MW magnetic field inside the cylindrical cavity of length L and radius R operating at TE_{011} mode are [28]:

$$\begin{cases} B_{1\rho} \sim -J_0'\left(\frac{v_{01}\rho}{R}\right)\sin\frac{\pi z}{L} \\ B_{1\varphi} = 0 \\ B_{1z} \sim J_0\left(\frac{v_{01}\rho}{R}\right)\cos\frac{\pi z}{L}, \end{cases} \tag{7}$$

where $J_0'(v)$ is the first derivative of $J_0(v)$, $v_{01} = 3.832$ is the first root of $J_0'(v)$. Assuming small filling factor, we can neglect the change of $\boldsymbol{B}_1$ distribution in the presence of the crystal sample. A small crystal sample is placed at the center of the cavity ($\rho = 0, z = 0$), where MW magnetic field is the most homogeneous. There only z component of $\boldsymbol{B}_1$ is essential in Eq. (7). Rabi frequency $\Omega_R(\boldsymbol{r})$ of Cr^{5+} ion placed at the point $\boldsymbol{r}(\rho, z, \varphi)$ in the sample is given by the relation $\Omega_R(\boldsymbol{r}) = g_\perp \mu_B B_1(\boldsymbol{r})/(2\hbar)$. The number of spins involved in transient nutations at the point $\boldsymbol{r}$ is proportional to $\Omega_R(\boldsymbol{r})$. We make a reasonable suggestion that Cr^{5+} ions have a random spatial distribution in the crystal not correlated to their spectral position within the ESR line. Then, instead of Eq. (5), $\langle S_{\|}(t)\rangle$ is given now by the following integral over the sample volume V_0:

$$\begin{aligned}\langle S_{\|}(t)\rangle &\sim \int_{V_0} \Omega_R(\boldsymbol{r}) j_0(\Omega_R(\boldsymbol{r})t)dV \\ &\simeq \Omega_R \int_{V_0} j_0\left(J_0\left(\frac{v_{01}\rho}{R}\right)\cos\frac{\pi z}{L}\cdot\Omega_R t\right)dV,\end{aligned} \tag{8}$$

where we write henceforth $\Omega_R \equiv \Omega_R(\boldsymbol{r} = 0)$. Since the sample dimensions are small compared to those of the resonator:

$$J_0\left(\frac{v_{01}\rho}{R}\right) \simeq 1 - \frac{1}{4}\left(\frac{v_{01}\rho}{R}\right)^2, \quad \cos\frac{\pi z}{L} \simeq 1 - \frac{1}{2}\left(\frac{\pi z}{L}\right)^2,$$

$$\langle S_{\|}(t)\rangle \sim \int_{V_0} j_0\left(\left(1 - \left(\frac{v_{01}\rho}{2R}\right)^2 - \left(\frac{\pi z}{\sqrt{2}L}\right)^2\right)\Omega_R t\right)dV.$$

Now let us introduce dimensionless variables $\tilde{\rho} = \frac{v_{01}\rho}{2R}$, $\tilde{z} = \frac{\pi z}{\sqrt{2}L}$, change to spherical coordinates (r, θ, α), with $r^2 = \tilde{\rho}^2 + \tilde{z}^2$, and integrate over θ, α:

$$\langle S_{\|}(t)\rangle \sim \int_0^\infty j_0((1-r^2)\Omega_R t)\Theta(r)r^2 dr,$$

where $r^2\Theta(r)$ is the area of the sample spherical surface at radius r. Obviously, the spherical angle $\Theta(r) = 4\pi$ for $0 \leqslant r \leqslant r_0$, and $\Theta(r) = 0$ for $r > r_{max}$, with $r_0 < r_{max} \ll 1$ being minimal (r_0) and maximal (r_{max}) dimensionless radii of the sample. At $r_0 < r \leqslant r_{max}$ the function $\Theta(r)$ gradually declines from 4π to 0. Its exact form in that range depends on the shape of the sample and is inessential in our schematic calculations. We assume $\Theta(r) \simeq 4\pi e^{-r^2/r_{max}^2}$ in the whole range $0 \leqslant r < \infty$, the form that roughly meets the above criteria. Employing Eq. (6), we obtain in the limit $\Omega_R t \gg 1$:

$$\langle S_{\|}(t)\rangle \sim (1+(\pi\Omega_R t)^2)^{-1/4}\int_0^\infty \cos\left((1-r^2)\Omega_R t + \frac{\pi}{4}\right)e^{-r^2/r_{max}^2}r^2 dr.$$

The integration yields

$$\langle S_{\|}(t)\rangle \approx \begin{cases} S_0(t)\cos(\Omega_R t + \pi/4), & 1 \ll \Omega_R t \ll r_{max}^{-2} \\ S_0(t)\cos(\Omega_R t - \pi/2), & \Omega_R t \gg r_{max}^{-2}, \end{cases} \tag{9}$$

where the amplitude of oscillations equals

$$S_0(t) = S_0(0)\left(1 + (\pi\Omega_R t)^2\right)^{-1/4}\left(1 + (r_{\max}^2\Omega_R t)^2\right)^{-3/4}. \quad (10)$$

It means that at $\Omega_R t \gg r_{\max}^{-2}$ the damping of longitudinal magnetization follows the polynomial time dependence $(\Omega_R t)^{-2}$. It is easy to show that at conditions $r_{\max} \ll 1$, $r_{\max}^2\Omega_R t \gg 1$ assumed above the asymptotic behavior $\sim(\Omega_R t)^{-2}$ is independent of the exact form of $\Theta(r)$.

In the case of weak broadening $\sigma \ll \Omega_R$, we replace j_0 in Eq. (8) by cosine and similarly get

$$S_0(t) = S_0(0)(1 + (r_{\max}^2\Omega_R t)^2)^{-3/4}, \quad \Omega_R t \gg 1. \quad (11)$$

Thus, in this case the decay pattern of RO after a number of oscillations also becomes polynomial, with the amplitude $\sim(\Omega_R t)^{-3/2}$.

Provided with the dimensions of the sample and the resonator used in experiments, we can calculate the decay function of RO more precisely. Our *W*-band measurements were carried out at MW frequency of 93.9 GHz using standard Bruker *W*-band cylindrical resonator with $L \approx 3$ mm, $R \approx 2.3$ mm operating at TE_{011} mode. A quartz tube of 0.5 mm in diameter contained the crystal sample in the form of a thin rod with approximate dimensions $l_x \times l_y \times l_z = 0.3 \times 0.3 \times 1$ mm. The tube was placed at the center of the resonator parallel to its *z*-axis. The distribution of the MW magnetic field amplitude $B_1(\boldsymbol{r})$ calculated by Eq. (7) at the cross-section of the sample containing *z*-axis is shown in Fig. 5. $B_1(\boldsymbol{r})$ is maximal at the center of the sample ($r = 0$) and decreases to 0.84 $B_1(0)$ at the edges.

The inhomogeneous width of the central ESR line at *W* band is ~10 G, thus the condition $\sigma > \Omega_R$ in our measurements is justified (see Fig. 3). The numeric integration over the sample volume in Eq. (8) gives $\langle S_{\|}(t)\rangle$ dependence which is in good agreement with the experimental one (see Fig. 3). Also, the predicted phase shift of $3\pi/4$ between the oscillations in the range $1 \ll \Omega_R t \ll r_{\max}^{-2}$ and $\Omega_R t \gg r_{\max}^{-2}$ (Eq. (9)) manifests itself in experimentally observed gradual decrease of their period from the initial 88 ns at $t = 0$ down to 75 ns.

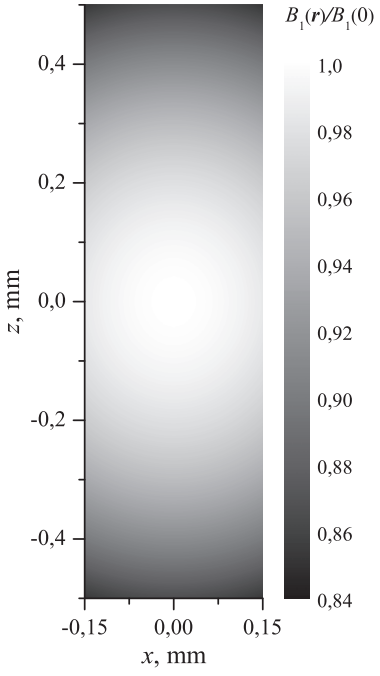

Fig. 5. $B_1(\boldsymbol{r})$ distribution inside the crystal sample used in *W*-band experiments, calculated according to Eq. (7). The gray scale represents the fraction $B_1(\boldsymbol{r})/B_1(0)$, where $B_1(0)$ denotes the MW field amplitude at the center of the cavity.

To obtain the characteristic damping time of RO, we fit the amplitude of RO to Lorentzian $\langle S_{\|}(0)\rangle(1 + (t/\tau_R)^2)^{-1}$. This form is more appropriate to our model (Eq. (10)) than the exponential $\langle S_{\|}(0)\rangle e^{-\tau_R/t}$ one used in previous works [4,6]. The resultant fitting curve (dashed line in Fig. 3) corresponds to $\tau_R = 105$ ns.

In order to check the validity of Eq. (1), RO measured at different intensities of MW field were obtained at the central ESR line of *W* band. The resultant $\tau_R^{-1}(\Omega_R)$ dependence depicted in Fig. 6 is linear: $\tau_R^{-1} = \beta\Omega_R$, with $\beta = 0.11$. Since $T_M^{-1} \ll \beta\Omega_R$, the first term of Eq. (1) is indistinguishable. Thus, phase relaxation of Cr^{5+} ions does not affect the decay of transient nutations and was neglected in our calculations. The peculiar linear dependence of τ_R^{-1} on Ω_R is simply explained by the fact that all the equations in the above model contain variables t and Ω_R as the product $\Omega_R t$. It follows from Eqs. (9) and (10) that

$$\langle S_{\|}(t)\rangle \sim (1 + (\pi\Omega_R t)^2)^{-1/4}(1 + (\beta\Omega_R t)^2)^{-3/4}\sin(\Omega_R t), \quad \Omega_R t \gg r_{\max}^{-2}, \quad (12)$$

where $r_{\max}^2 \approx \beta = 0.11$. Thus, we obtain a rough estimate $r_{\max} \approx 0.33$. It is in good agreement with $r_{\max} = \sqrt{v_{01}^2(l_x^2 + l_y^2)/16R^2 + \pi^2 l_z^2/8L^2} = 0.41$ derived from the actual size, shape and orientation of the crystal sample in the cavity. More elaborate calculations involving numeric integration in Eq. (8) provide even better agreement between the calculated and detected decays of Rabi oscillations, as seen in Fig. 3.

Note that the observed decay of RO is not an artifact of our experimental setup. In case of microwave cavities, the spatial distribution of $\boldsymbol{B}_1$ amplitude is formed by standing waves inside the resonator and thus experimentally unavoidable.

As another example of strong line broadening, we re-examined the results of our previous work on $CaWO_4$:Yb^{3+} [6] and found that after a number of oscillations the transient nutations of Yb^{3+} ion at *X* and *W* bands follow the expected decay pattern $(\Omega_R t)^{-2}$.

In order to investigate the RO decay pattern in the case of weak line broadening, measurements of RO were carried out at low-frequency *S* band. Here the inhomogeneous width of the central ESR line is only ~0.25 G, thus satisfying the condition $\sigma \ll \Omega_R$ in the experimental range of Ω_R. Due to MW wavelength of 8.5 cm, conventional cylindrical or rectangular cavities at *S* band become cumbersome. Lumped-element resonators with smaller physical size at low frequencies are preferable. As compared to conventional resonant cavities, they provide higher filling factors thus

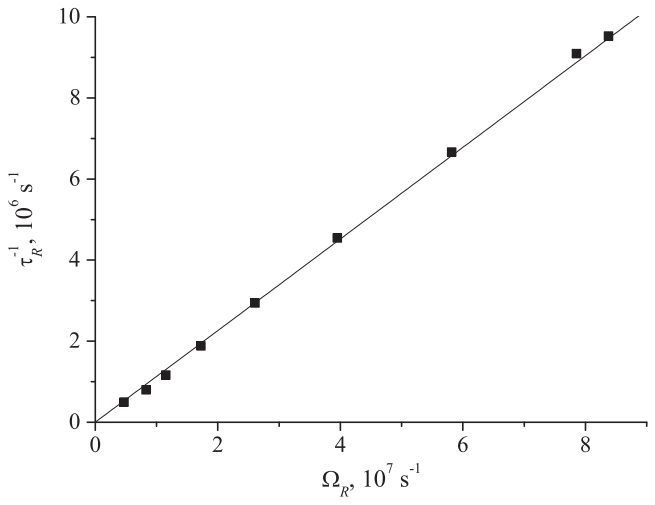

Fig. 6. Dependence of RO decay time on Rabi frequency, $\tau_R^{-1}(\Omega_R)$, derived from the measurements of Rabi oscillations at the central ESR line of *W* band (squares), the linear fit $0.11 \cdot \Omega_R$ (solid line). $T = 6$ K.

enabling to use smaller samples. In our *S*-band measurements, we used four-loop, four-gap cylindrical bridged loop-gap resonator (BLGR [29]) with 5.5 mm loop diameter and 10 mm length (see Fig. 7). It produced axially oriented MW magnetic field $B_{1z}(\boldsymbol{r})$ and was tuned to MW frequency of 3.53 GHz. The detailed description of the particular *S*-band spectrometer can be found in [30]. A quartz tube containing the crystal sample with dimensions $l_x \times l_y \times l_z = 1.4 \times 2.8 \times 2.4$ mm was placed at the center of BLGR where the MW magnetic field homogeneity is maximal. The measured RO exhibit very slow damping, where more than 100 oscillations are distinguishable (see Fig. 4A). Since RO at *S* band are observed at t comparable to T_M, the phase relaxation here is not negligible and must be taken into account in the above model. We assume that $\sigma \ll \Omega_R$, thus nutation frequencies of different Cr^{5+} ions in the ESR line are almost identical. The Hamiltonian of magnetic dipolar interaction between two chromium ions in the case of magnetic isotropy $g_\parallel \approx g_\perp \approx g_e = 2$ equals

$$H_{12} = \frac{g_e^2\mu_B^2}{r^3}\left\{(\boldsymbol{S}_1\cdot\boldsymbol{S}_2) - \frac{3(\boldsymbol{S}_1\cdot\boldsymbol{r})(\boldsymbol{S}_2\cdot\boldsymbol{r})}{r^2}\right\}, \tag{13}$$

where $\boldsymbol{S}_1$, $\boldsymbol{S}_2$ are the spins of the two ions, $\boldsymbol{r}(x, y, z)$ is the radius-vector connecting the ions.

Rewriting Eq. (13) in the same rotating reference frame (RRF) used in the calculations above and preserving only time-independent terms, we obtain

$$H_{12}^{RRF} = \frac{g_e^2\mu_B^2}{r^3}(1 - 3\cos^2\theta_{12})\left\{S_{1z}S_{2z} - \frac{1}{2}(S_{1x}S_{2x} + S_{1y}S_{2y})\right\}, \tag{14}$$

with $\cos\theta_{12} = z/r$. We have chosen the system of coordinates in RRF such that the fields $\boldsymbol{B}_0$ and $\boldsymbol{B}_1$ are aligned along z and x axes, respectively. Accounting for the term $\sim S_{1z}S_{2z}$ in Eq. (14), we obtain the shift of Larmor frequency of the first ion due to its interaction with the second ion

$$\Delta\omega_{12} = \frac{g_e^2\mu_B^2}{r^3}(1 - 3\cos^2\theta_{12})S_{2z}. \tag{15}$$

Performing summation over all spins and averaging over the spin spatial distribution in the crystal, one obtains the rms shift of Larmor frequency $\Delta\omega_d$ [23]. That causes the static broadening of ESR line with the half-width $\Delta\omega_d$. Accounting for the term $\sim S_{1x}S_{2x}$ in Eq. (14) and following the same procedure, we obtain that the rms shift of Rabi frequency of Cr^{5+} ion equals $\kappa\Delta\omega_d/2$ (only κth part of the spins corresponding to excited ESR line undergo nutations and thus their time-averaged magnetization along the x axis in RRF is non-zero). The value of $\kappa\Delta\omega_d/2$ corresponds to the half of the first term in Eq. (3) and to $T_M^{-1}/2$ in Eq. (1). Thus, now we can correct our Eq. (8) for RO decay introducing phase relaxation factor $e^{-\kappa\Delta\omega_d t/2}$ and substituting cosine for j_0:

$$\langle S_\parallel(t)\rangle \sim e^{-\kappa\Delta\omega_d t/2}\int_{V_0}\Omega_R(\boldsymbol{r})\cos(\Omega_R(\boldsymbol{r})t)dV. \tag{16}$$

The MW magnetic field inhomogeneity inside BLGR arises mainly from the gaps in its metallic layer. Unfortunately, we have not accomplished the detailed measurement of $\boldsymbol{B}_1(\boldsymbol{r})$ distribution inside the BLGR. However, the approximation of the data obtained from similar resonators [31–33] provides us with an estimate of 0.96 $B_1(0)$ at the edges of the crystal sample in the xy plane of BLGR. Roughly, we can assume cosine distribution of the MW magnetic field amplitude in the xy plane: $B_{1z}(\rho) = B_{1z}(0)\cos(k\rho)$, $\rho = \sqrt{x^2 + y^2}$, with the parameter k corresponding to 96% MW field homogeneity inside the sample. After numeric integration in Eq. (16) we obtain the decay pattern depicted in Fig. 4B. The slight superimposed modulations of the amplitude of RO seen in Fig. 4A and B originate from the beating of the magnetization from the center of the crystal sample (where the field homogeneity is highest) and from its edges.

In order to obtain characteristic damping time of RO, we use the fit to the function $\langle S_\parallel(0)\rangle e^{-\kappa\Delta\omega_d t/2}(1 + (t/\tau_R)^2)^{-3/4}$, in accord with Eq. (11). The resultant dependence corresponding to $\tau_R \approx 2.2$ μs is represented by the dashed line in Fig. 4A. The measurements of RO amplitude decays at different values of Ω_R were successfully approximated by the expression $\langle S_\parallel(0)\rangle e^{-\kappa\Delta\omega_d t/2}(1 + (\beta\Omega_R t)^2)^{-3/4}$, with $\beta = 0.009$.

Finally, we would like to draw comparison between our model of decay of Rabi oscillations and the stochastic semi-phenomenological model of Shakhmuratov et al. [14,15]. In their model, they suggest that in the presence of resonant external MW magnetic field $B_1 e^{-i\omega_0 t}$ in the crystal also appears additional stochastic component transverse to $\boldsymbol{B}_0$ and with the amplitude proportional to B_1, namely, $B_1(\theta_1(t) + i\theta_2(t))e^{-i\omega_0 t}$ [14]. Further, under assumptions $\sigma > \Omega_R, T_M^{-1}$, they arrive to the term $\beta\Omega_R$ in Eq. (1). Since the parameter β in their measurements [15] appears to depend on the concentration of paramagnetic impurity, they ascribe the stochastic magnetic field to MD interactions between paramagnetic ions.

Let us estimate the contribution of MD interactions to such stochastic field in our case. It is the same fluctuating local magnetic field that causes the damping of Rabi oscillations with the rate $\kappa\Delta\omega_d/2$ in the weak broadening case $\sigma \ll \Omega_R$ (Eq. (16)). The derivation of the analogous contribution in the strong broadening case $\sigma > \Omega_R$ is straightforward. Roughly, only the part of spins $\sim\Omega_R/\sigma$ in the ESR line undergo rotations when the resonant MW field is applied and thus contribute to the transverse stochastic field. Following the same argumentation as in Eqs. (13)–(15), we obtain the contribution to the damping rate of Rabi oscillations due to MD interactions: $\tau_{R(d)}^{-1} \approx \kappa\Delta\omega_d\Omega_R/2\sigma$. That gives

$$\beta_{(d)} \approx \kappa\Delta\omega_d/2\sigma = \frac{2\pi^2\kappa C g_\perp^2\mu_B^2}{9\sqrt{3}\sigma h}. \tag{17}$$

For the central ESR line of *W* band $\beta_{(d)} = 3 \times 10^{-4}$, which is nearly 400 times less than the value of $\beta_{(MW)} = 0.11$ calculated for $CaWO_4:Cr^{5+}$ crystal in the framework of our MW field inhomogeneity model.

The concentration dependence of β is an arguable question. When MD mechanism of the damping dominates (i.e. $\beta_{(d)} \gg \beta_{(MW)}$), one expects linear dependence of β on spin concentration C (Eq. (17)). The earlier studies [13] of E' centers in glassy silica and of $[AlO_4]^0$ centers in quartz suggested that β is concentration independent. However, later measurements [15] of E' centers revealed $\beta \sim C$. The estimates of $\beta_{(d)}(C)$ for E' centers according to Eq. (17) are a few times lower than the actual values of $\beta(C)$ [15]. More

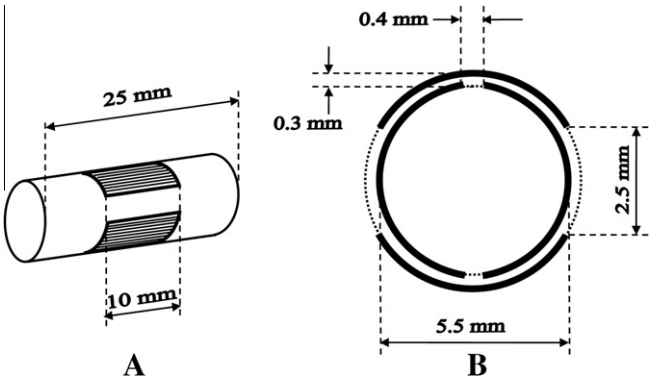

Fig. 7. A – a side view, B – a cross-section of four-loop, four-gap cylindrical bridged loop-gap resonator (BLGR) used in the *S*-band measurements. Its resonant structure is formed by four thin metallic layers of 10 mm length adjusted to the inner and outer surfaces of a cylindrical quartz support (25 mm length and 5.5 mm inner diameter).

accurate estimates of $\beta_{(d)}$ together with the interpretation of the dependence $\beta(C)$ measured in [13,15] will be presented in a separate paper. The underestimation $\beta_{(d)} \ll \beta$ takes place also in case of V_{15} [10], although the authors of [10] claim that MD interactions between different V_{15} molecular magnets are responsible for the damping of Rabi oscillations in the specific range of Ω_R. Thereby, we doubt the assertion that the term $\beta\Omega_R$ in Rabi decay rate in [13–15,10] is caused only by MD interactions between paramagnetic impurities.

There are at least two experimental confirmations indicating that the stochastic model [14,15] is inadequate in the case of $CaWO_4$:Cr^{5+} crystal samples used in the present work. Firstly, in order to investigate the dependence of τ_R on the concentration of paramagnetic ions, we measured RO decays of odd chromium isotopes at *S* and *W* bands. The obtained values of τ_R were comparable to those of the central ESR line, in agreement with the fact that the contribution $\beta_{(MW)}$ in β is concentration independent. Secondly, as was mentioned above, the stochastic model [14,15] is valid only when $\sigma > \Omega_R$. However, we observed and successfully explained the decay of Rabi oscillations even when $\sigma \ll \Omega_R$ (*S* band). Both these facts indicate that, at least for the given crystal samples and under the specified experimental conditions, the decay of Rabi oscillations is induced by MW field inhomogeneity inside the resonator.

3. Conclusions

In the present work we have investigated decoherence processes responsible for the reduction of the number of coherent single-qubit operations Q_M of Cr^{5+} ions in $CaWO_4$ single crystal (0.0006 at.% Cr^{5+}). Comparison of the experimental and calculated phase memory times T_M revealed that phase relaxation of Cr^{5+} ions at liquid helium temperatures is mostly caused by instantaneous diffusion. Since the impact of ID on T_M is concentration-dependent, larger Q_M values can be achieved for the crystals with lower Cr^{5+} concentrations.

The decay of Rabi oscillations under specific experimental conditions was found to be mostly due to intrinsic spatial distribution of MW magnetic field intensity inside the crystal sample. All of the following distinctive features observed experimentally were successfully explained in the framework of our RO decay model: (1) essentially non-exponential, rather polynomial RO damping pattern; (2) linear dependence of characteristic damping times on Rabi frequency; (3) the superimposed modulations of RO amplitude at *S* band; (4) characteristic damping times do not depend on the concentration of paramagnetic impurity. In both cases – weak (*S* band) and strong (*W* band) ESR line broadening – the calculated RO decays very well agree with experimental data. We hope that the obtained results can avail in future studies of Rabi oscillations in magnetically diluted solids. Bridged loop-gap resonators and smaller crystal samples are suggested to increase MW field homogeneity inside the sample. Furthermore, it is possible to use BB1 composite pulses to get rid of the damping of Rabi oscillations due to MW field inhomogeneity [28].

The possible future implementations of diamagnetic solids with paramagnetic impurities in quantum computation will require selective address to a single spin. The MW field inhomogeneity causes mutual dephasing of magnetizations of spins located at different points in the crystal. Therefore, the observed RO decay does not in principle affect Q_M since during the transient nutations each single spin state remains coherent. However, the results obtained in the present work will help to separate relaxational and "inhomogeneous" parts of experimental decay rates of Rabi oscillations in future studies. In particular, we believe that the model developed here can at least partly explain recent observations of anomalous damping of Rabi oscillations in various magnetically diluted solids.

4. Experimental

The sample of $CaWO_4$ single crystal with 0.0006 atomic% Cr^{5+} (7.6×10^{16} ions/cm^3) was grown by the Czochralski method in Magnetic Resonance Laboratory of Kazan State University by N.A. Karpov.

Measurements of continuous-wave and echo-detected ESR spectra were performed using Bruker Elexsys E680 *W*-band and home-built *S*-band [30] pulse spectrometers at temperatures 3–30 K with both static magnetic field $\boldsymbol{B}_0$ and MW field $\boldsymbol{B}_1$ perpendicular to the crystal *c* axis. In all experiments, the lengths of $\pi/2$ pulses were 24 and 28 ns for *S* and *W* bands, respectively. Measurements of T_1, T_M and τ_R were performed mostly at central ESR line. However, in order to investigate how the reduction of Cr^{5+} ion concentration would affect the coherence times, some data were obtained at high- and low-field hyperfine components.

The spin–lattice relaxation times T_1 were obtained through an inversion-recovery pulse sequence $\pi - \tau'$ followed by spin-echo sequence $\pi/2 - \tau - \pi$ – echo. There τ' was incremented and τ kept fixed (240 and 8000 ns for *S* and *W* bands, respectively).

The phase memory times T_M of Cr^{5+} ion in $CaWO_4$ crystal were detected through two-pulse Hahn spin-echo sequence $\pi/2 - \tau - \pi$ – echo.

RO were recorded through the following pulse sequence: nutation pulse *t* – delay – $\pi/2 - \tau - \pi$ – echo. There the nutation pulse of length *t* was followed by a delay longer than T_M in order to get rid of transverse component of the average magnetization. After that, the remaining longitudinal spin component $\langle S_{||}(t)\rangle$ parallel to $\boldsymbol{B}_0$ was obtained after two-pulse echo sequence.

Acknowledgments

This work was partially supported by RFBR (Grant N09-02-00930) and by Dynasty Foundation. The authors are grateful to B.Z. Malkin for advice and fruitful discussions of the results, to T.F. Prisner for the possibility to perform *S*-band measurements and to A.A. Rodionov for the help in concentration measurements.

References

[1] D.P. DiVincenzo, Quantum computation, Science 270 (1995) 255–261.
[2] R. Vrijen, E. Yablonovitch, K. Wang, H.W. Jiang, A. Balandin, V. Roychowdhury, T. Mor, D. DiVincenzo, Electron-spin-resonance transistors for quantum computing in silicon-germanium heterostructures, Phys. Rev. A 62 (2000) 012306.
[3] F.H.L. Koppens, C. Buizert, K.J. Tielrooij, I.T. Vink, K.C. Nowack, T. Meunier, L.P. Kouwenhoven, L.M.K. Vandersypen, Driven coherent oscillations of a single electron spin in a quantum dot, Nature 442 (2006) 766–771.
[4] S. Bertaina, S. Gambarelli, A. Tkachuk, I.N. Kurkin, B. Malkin, A. Stepanov, B. Barbara, Rare-earth solid-state qubits, Nat. Nanotechnol. 2 (2007) 39–42.
[5] S. Bertaina, J.H. Shim, S. Gambarelli, B.Z. Malkin, B. Barbara, Spin-orbit qubits of rare-earth-metal ions in axially symmetric crystal fields, Phys. Rev. Lett. 103 (2009) 226402.
[6] R.M. Rakhmatullin, I.N. Kurkin, G.V. Mamin, S.B. Orlinskii, M.R. Gafurov, E.I. Baibekov, B.Z. Malkin, S. Gambarelli, S. Bertaina, B. Barbara, Coherent spin manipulations in Yb^{3+}:$CaWO_4$ at *X*- and *W*-band EPR frequencies, Phys. Rev. B 79 (2009) 172408.
[7] S. Bertaina, L. Chen, N. Groll, J. Van Tol, N.S. Dalal, I. Chiorescu, Multiphoton coherent manipulation in large-spin qubits, Phys. Rev. Lett. 102 (2009) 050501.
[8] C. Schlegel, J. van Slageren, M. Manoli, E.K. Brechin, M. Dressel, Direct observation of quantum coherence in single-molecule magnets, Phys. Rev. Lett. 101 (2008) 147203.
[9] S. Bertaina, S. Gambarelli, T. Mitra, B. Tsukerblat, A. Müller, B. Barbara, Quantum oscillations in a molecular magnet, Nature 453 (2008) 203–206.
[10] J.H. Shim, S. Gambarelli, S. Bertaina, T. Mitra, B. Tsukerblat, A. Müller, B. Barbara, Driven spin-bath decoherence in the molecular magnet V_{15}, arXiv:1006.4960v2.
[11] S. Nellutla, K.-Y. Choi, M. Pati, J. van Tol, I. Chiorescu, N.S. Dalal, Coherent manipulation of electron spins up to ambient temperatures in Cr^{5+} ($S = 1/2$) doped K_3NbO_8, Phys. Rev. Lett. 99 (2007) 137601.

[12] I.I. Rabi, Space quantization in a gyrating magnetic field, Phys. Rev. 51 (1937) 652–654.
[13] R. Boscaino, F.M. Gelardi, J.P. Korb, Non-Bloch decay of transient nutations in S = 1/2 systems: an experimental investigation, Phys. Rev. B 48 (1993) 7077–7084.
[14] R.N. Shakhmuratov, F.M. Gelardi, M. Cannas, Non-Bloch transients in solids: free induction decay and transient nutations, Phys. Rev. Lett. 79 (1997) 2963–2966.
[15] S. Agnello, R. Boscaino, M. Cannas, F.M. Gelardi, R.N. Shakhmuratov, Transient nutations decay: the effect of field-modified dipolar interaction, Phys. Rev. A 59 (1999) 4087–4090.
[16] R.M. Hazen, L.W. Finger, J.W.E. Mariathasan, High-pressure crystal chemistry of scheelite-type tungstates and molybdates, J. Phys. Chem. Solids 46 (1985) 253–263.
[17] R.W. Kedzie, J.R. Shane, M. Kestigian, EPR observation of anomalous saturation behavior due to T_1 limited spin packet linewidths in $CaWO_4$:Cr^{5+}, Phys. Lett. 11 (1964) 286–289.
[18] K.V. Lingam, P.G. Nair, B. Venkataraman, Electron spin resonance of Cr^{5+} in $CaWO_4$, Proc. Ind. Acad. Sci. 70 (1969) 29–41.
[19] B.Z. Malkin, Crystal field and electron–phonon interaction in rare-earth ionic paramagnets, in: A.A. Kaplyanskii, R.M. Macfarlane (Eds.), Spectroscopy of Solids Containing Rare Earth Ions, North-Holland, Amsterdam, 1987, pp. 13–50.
[20] A. Abragam, B. Bleaney, Electron Paramagnetic Resonance of Transition Ions, Oxford Univ. Press, London, 1970.
[21] I.N. Kurkin, Yu.K. Chirkin, V.I. Shlenkin, Investigation of relaxational characteristics of Cr^{5+} ions in $CaMoO_4$ monocrystals, Sov. Phys. Solid State 17 (1975) 2028–2032.
[22] A. Senyshyn, H. Kraus, V.B. Mikhailik, V. Yakovyna, Lattice dynamics and thermal properties of $CaWO_4$, Phys. Rev. B 70 (2004) 214306.
[23] W.B. Mims, Phase memory in electron spin echoes, lattice relaxation effects in $CaWO_4$: Er, Ce, Mn, Phys. Rev. 168 (1968) 370–389.
[24] K.M. Salikhov, S.A. Dzuba, A.M. Raitsimring, The theory of electron spin-echo signal decay resulting from dipole–dipole interactions between paramagnetic centers in solids, J. Magn. Res. 42 (1981) 255–276.
[25] A. Abragam, The Principles of Nuclear Magnetism, Clarendon Press, Oxford, 1961.
[26] J.J.L. Morton, A.M. Tyryshkin, A. Ardavan, K. Porfyrakis, S.A. Lyon, G.A.D. Briggs, Measuring errors in single-qubit rotations by pulsed electron paramagnetic resonance, Phys. Rev. A 71 (2005) 012332.
[27] J.J.L. Morton, A.M. Tyryshkin, A. Ardavan, K. Porfyrakis, S.A. Lyon, G.A.D. Briggs, High fidelity single qubit operations using pulsed electron paramagnetic resonance, Phys. Rev. Lett. 95 (2005) 200501.
[28] Ch.P. Poole, Electron Spin Resonance: A Comprehensive Treatise on Experimental Techniques, Wiley, New York, 1983.
[29] S. Pfenninger, J. Forrer, A. Schweiger, Bridged loop-gap resonator: a resonant structure for pulsed ESR transparent to high-frequency radiation, Rev. Sci. Instrum. 59 (1968) 752.
[30] A. Weber, M. Rohrer, J.T. Törring, T.F. Prisner, A CW and pulsed S-band spectrometer, in: D. Ziessow, W. Lubitz, F. Lendzian (Eds.), Proceedings of the 29th Congress AMPERE/13th ISMAR, vol. 2, 1998, pp. 1138. A Brief Description of the Spectrometer is also Available at <http://www.prisner.de/Activities/Research/Equipment/S-Band/s_band_spectrometer.shtml>.
[31] S. Petryakov, M. Chzhan, A. Samouilov, G. He, P. Kuppusamy, J.L. Zweier, A bridged loop-gap S-band surface resonator for topical EPR spectroscopy, J. Magn. Res. 151 (2001) 124–128.
[32] J. Forrer, S. Pfenninger, G. Sierra, G. Jeschke, A. Schweiger, B. Wagner, Th. Weiland, Probeheads and instrumentation for pulse EPR and ENDOR spectroscopy with chirped radio frequency pulses and magnetic field steps, Appl. Magn. Res. 10 (1996) 263–279.
[33] M. Ono, A. Suenaga, H. Hirata, Experimental investigation of RF magnetic field homogeneity in a bridged loop-gap resonator, Magn. Res. Med. 47 (2002) 415–419.